Observation of Saturation of Fidelity Decay with an Atom Interferometer

Citation

Published Version

Permanent link

Terms of Use

Share Your Story

Observation of Saturation of Fidelity Decay with an Atom Interferometer

Saijun Wu,* Alexey Tonyushkin, and Mara G. Prentiss

Department of Physics, Harvard University, Cambridge, Massachusetts 02138, USA
(Received 21 February 2008; published 16 July 2009)

We use an atom interferometer to investigate the dynamics of matter waves in a periodically pulsed optical standing wave: an atom optics realization of the quantum kicked rotor that exhibits chaotic classical dynamics. We experimentally show that a measure of the coherence between the interferometer diffraction orders can revive after a quick initial loss, and can approach a finite asymptote as the number of kicks increases. This observation demonstrates that quantum fidelity of a classically chaotic system can survive strong perturbations over long times without decay.

In a seminal paper [1], Asher Peres demonstrated that quantum states of classically chaotic systems are more fragile to perturbations than those with regular classical motion. In the paper he also suggested using the decay of fidelity, $F(t) = |\langle \psi | \hat{U}'(t)^{-1} \hat{U}(t) | \psi \rangle|^2$ with $\hat{U}(t) = e^{-i\hat{H}t}$, $\hat{U}'(t) = e^{-i(\hat{H}+\delta\hat{V})t}$, and $\hat{H}$ the Hamiltonian, to study the stability of a quantum trajectory $\hat{U}(t)|\psi\rangle$ under a perturbation $\delta\hat{V}$. More recently, the Lyapunov exponents of classically chaotic systems have been found to determine a perturbation-independent rate of fidelity decay [2]. These discoveries shed light on the fundamental problem concerning quantum irreversibility and classical chaos. From a practical point of view, however, an exponential decay of quantum fidelity requires exponentially high precision for longtime quantum control. Thus an outstanding question is whether precise quantum control could be practically implemented in complex systems that exhibit classical chaos. Fortunately, as fragile as quantum states are, classical instabilities do not always represent the instability of quantum systems: for certain types of perturbations, it was shown that quantum trajectories of classically chaotic systems maintain a constant overlap with their perturbation-free copies for a very long time [3–5]. Related to wave localization phenomena, such "freeze" or "saturation" of fidelity decay is understandable only when the system is treated fully quantum mechanically as our semiclassical intuition breaks down.

Decay of quantum fidelity can be studied with an interferometer [5–8]. To see this, consider two quantum trajectories in a 3-grating atom interferometer sequence [9] and a potential $\hat{V}$ applied during $0 < t < T$ [Fig. 1(a)]. With the "mirror" diffraction at $t = T$ to reverse the relative momentum of the two trajectories, the overlap of the two trajectories at $t = 2T^+$ measures the fidelity for a quantum trajectory evolving in the potential $\hat{V}$ under a momentum displacement perturbation, written as $\delta\hat{V}(t) \equiv \hat{V} - \hat{D}^{-1}\hat{V}(t)\hat{D}$. Here $\hat{D} = e^{iQ\hat{x}}$ is a momentum displacement operator that corresponds to an atomic recoil due to a grating diffraction, Q is the k vector of the grating, and $\hat{x}$, $\hat{p}$ are the position and momentum operators. More

formally, with $|\psi(t)\rangle = \hat{U}_1(t)|\psi\rangle$ and $|\psi'(t)\rangle = \hat{U}_1(t)\hat{D}|\psi\rangle$ to label the "original" and the "displaced" trajectories during $0 < t < T$, the overlap at $t = 2T^+$ can be written as a fidelity amplitude $f = \langle \psi | \hat{U}_2(T)^{-1} \hat{U}_1(T) | \psi \rangle$, with $\hat{U}_{1,2}(T) = \hat{T} e^{-i \int_0^T \hat{H}_{1,2} dt}$ ($\hat{T}$ the time-ordering operator). Here $\hat{H}_1 = \hat{V}(t)$ and $\hat{H}_2 = \hat{D}^{-1}\hat{V}(t)\hat{D}$, with $\hat{V}(t)$ written in the interaction picture, i.e., $\hat{x}(t) = \hat{x} + \hat{p}t/m$. In previous experimental studies or proposals [5–7] $\hat{D}$ corresponds to an internal-state population inversion.

In this Letter, we provide the first atom optical demonstration of persistent quantum fidelity in a classically chaotic potential in the presence of strong perturbations [5]. We choose the classically chaotic potential $\hat{V}(t)$ to be an atom optics realization of quantum δ-kicked rotor potential (AQKR) [10,11], which is delivered by a periodically pulsed optical standing wave (SW) to laser-cooled atoms. Inspired by a recent theoretical work [4], we use an atom interferometer [9] to investigate the stability of matter wave dynamics in AQKR, by measuring the coherence loss between the interfering paths or, equivalently, the fidelity decay due to a momentum displacement perturbation (Fig. 1). The kicked rotor system is a standard paradigm for studying quantum and classical chaos [11]. In our previous work [12], matter wave coherence was found intact if AQKR is timed to nullify the perturbation $\delta\hat{V}(t)$.
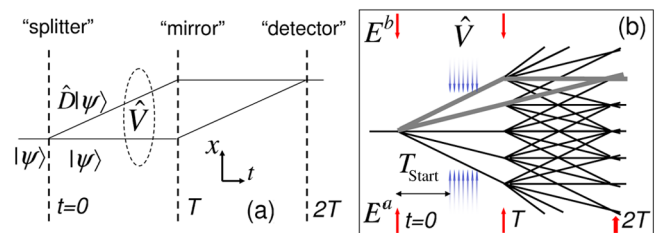

FIG. 1 (color online). (a) Schematic principle of measuring fidelity with an interferometer. Vertical dash lines represent three diffraction gratings. (b) Recoil diagram [24] of a matter wave grating echo interferometer perturbed by the AQKR potential $\hat{V}$. A representative interfering loop is marked with thick lines. The effect of diffractions due to $\hat{V}$ is not shown.

This Letter instead investigates the coherence loss over a wide range of perturbation strengths. When the repetition rate of AQKR matches the atomic recoil frequency (quantum resonance [13]), we find the matter wave coherence always saturates to a nonzero value, observable after as many as 150 kicks, after reviving from an initial loss. This effect (referred to as fidelity saturation) was predicted in the context of an internal-state atom interferometer setup [5]. It is worth noting that semiclassically the perturbation would lead to an exponential decay of fidelity to zero [4], since almost all classical trajectories of atoms are unstable under our typical experimental conditions [10,11].

We use the grating echo interferometer technique based on multipath interference effects [14,15]. The interference paths in Fig. 1(b) become easy to understand if we notice the multiple paths contributing to the interferometer signals form the same type of "loops." Specifically, an off-resonant SW diffraction at $t = 0$ produces matter waves in multiple orders weighted by $i^n J_n(\Theta)$ (Θ is the interferometer SW pulse area [14] and J_n is the nth order Bessel function). Adjacent diffraction orders, with their relative momentum reversed by the 2nd SW diffraction at $t = T$, form the smallest-area loops to interfere at $t = 2T$. We group loops of this type and plot the relative spatial displacement between the two paths with a δx-t "displacement diagram" in Fig. 2(a). The $\delta x = \delta x(t)$ lines in Fig. 2(a) will be referred to as "displacement lines," which guide peaks of the matter wave correlation function $W(P, X, t) = \mathrm{Tr}[\hat{\rho}(t)\hat{d}(P, X)]$ at $P = \pm\hbar Q$ and $X = \delta x(t) = \int_0^t \frac{P}{m} dt$ during free evolutions. Here $\hat{\rho}$ is the single atom density matrix operator, and $\hat{d}(P, X) = e^{i/\hbar(P\cdot\hat{x}-X\cdot\hat{p})}$ [16]. Spatially periodic matter wave density modulation appears whenever a displacement line crosses the $\delta x = 0$ axis. In particular, the interferometer output $\rho_{-Q} = W(-\hbar Q, X = 0)$ is the Fourier component of the density modulation at around $t = 2T$, which can be measured with a "grating echo" technique [14] by monitoring a Bragg-reflected light from one traveling mode of the SW, E^a, into the other (E^b).

The AQKR potential $\hat{V}$ [Figs. 1(b) and 2(b)] is generated with a pulsed SW similar to that used to make the interferometer. Pulsed at $t = \{T_i, i = 1 \ldots N\}$ with $T_i = T_{\mathrm{start}} + (i-1)T_{\mathrm{kick}}$, the AQKR potential can be written in the interaction picture as

(a)

$$\hat{V}(t) = \hbar\theta \cos[Q'\hat{x}(t)] \sum_{i=1}^{N} \delta(t - T_i). \quad (1)$$

Here the pulse area θ specifies the strength of each AQKR kick. The AQKR potential generally leads to an interferometer output $\tilde{\rho}_{-Q}$ with reduced amplitude [Fig. 2(b)]. The normalized amplitude $f \equiv \tilde{\rho}_{-Q}/\rho_{-Q}$ corresponds to a fidelity amplitude averaged over all the adjacent interferometer diffraction paths [Fig. 1(b)] in $\hat{V}(t)$ under the perturbation $\delta\hat{V}(t) = \hat{V}(t) - \hat{D}^{-1}\hat{V}(t)\hat{D}$. The strength of this perturbation can be characterized by a parameter $\phi_i = 2\theta \sin[Q'\delta x_0(T_i)/2]$ at each kick, with $\delta x_0(t) \equiv \hbar Q t/m$ [Fig. 2(b)] to be the displacement between pairs of interferometer paths. In particular, if $Q'\delta x_0(T_i) = 2n\pi$, i.e., if AQKR is pulsed only when the displacement is an integer multiple of the grating constant, the perturbation is nullified ($\phi_i = 0$) and no coherence loss is expected [12].

Here we use the displacement diagram in Fig. 2(b) to generally examine the interferometer coherence loss: The matter wave coherence that contributes to the interferometer signal is given by $W(P, X, t)$ along the original displacement line $\delta x_0(t)$. Thus f is equal to the fraction of the surviving coherence along $\delta x_0(t)$ after the AQKR interaction. It is easy to show that a SW impulse at t generally leads to [16]

$$W(P, X, t^+) = \sum_n J_n\left(2\theta \sin\frac{Q'X}{2}\right) W(P - n\hbar Q', X, t^-); \quad (2)$$

i.e., each SW kick corresponds to a "diffraction" of $W(P, X, t)$ by multiples of $\hbar Q'$ along its P axis, graphically leading to multiple displacement lines with different slopes on the $\delta x - t$ diagram. We iteratively apply Eq. (2) for each kick of AQKR at $t = T_i$ to obtain the fraction of the coherence surviving the AQKR interaction as

$$f = \sum_{\{n_i\}} \prod_{i=1}^{N} J_{n_i}[2\theta \sin(Q'X_i^{\{n_i\}}/2)]. \quad (3)$$

Here $X_i^{\{n_i\}} = \delta x_0(T_i) + s\frac{\hbar Q'}{m}T_{\mathrm{kick}}$ (with integer s) gives the displacement between a pair of diffraction orders during AQKR kicks. The sum is restricted to $\{n_i\}$ satisfying $\sum_i n_i = r_N = 0$, $\sum_i(i-1)n_i = s_N = 0$, which specifies the paths in the network of displacement lines [Fig. 2(b)] that begin and end with $\delta x_0(t) = \hbar Q t/m$.

Equation (3) can be significantly simplified when T_{kick} is chosen equal to an integer multiple of the half-Talbot time $T_{1/2} = \pi/\omega_{Q'}$ (quantum resonance), so that $X_i^{\{n_i\}} = \delta x_0(T_i)$, up to an integer multiple of kicked rotor SW grating constant. The parameter ϕ_i can then be used to characterize the perturbation strength for all pairs of paths represented by the displacement lines in Fig. 2(b) generated by AQKR, apart from the original displacement line $\delta x_0(t)$ generated by the first interferometer SW pulse. We rewrite the Bessel functions in integral form and perform
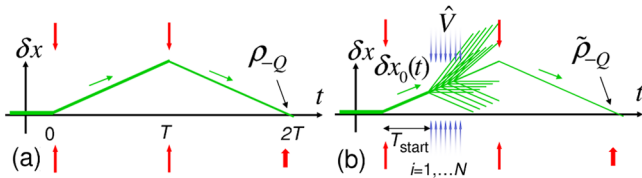
FIG. 2 (color online). (a) Diagram for the relative displacement between pairs of wave packets along the interfering loops of interest in Fig. 1(b). (b) Displacement diagram of the interferometer in the presence of AQKR potential $\hat{V}$.

the summation. If $Q \approx Q'$ so that $\phi_i \approx \phi = 2\theta \sin(\omega_Q T_{\text{start}})$ [17], Eq. (3) at quantum resonances can be written as

$$f_{\text{QR}}(\phi, N) = \frac{1}{2\pi} \int_{-\pi}^{\pi} J_0\left[\phi \frac{\sin(Ny/2)}{\sin(y/2)}\right] dy. \quad (4)$$

Equation (4) is remarkable: as suggested in Ref. [5], at the large N limit $f_{\text{QR}} = \int_{-\pi/2}^{\pi/2} J_0[\phi \sec(\alpha)/2]^2 d\alpha/\pi > 0$; i.e., matter wave fidelity always saturates to a nonzero value, in the presence of the perturbation with arbitrary strength ϕ and regardless of whether or not the AQKR dynamics are classically chaotic [18].

Below we will show that our experimental results are consistent with this theoretical prediction. The experimental setup is similar to that in Refs. [12,19,20]. Approximately 10^7 laser-cooled ^{87}Rb atoms in their ground state $F = 1$ hyperfine level are loaded into a magnetic guide oriented along $\mathbf{e_x}$, resulting in a cylindrically shaped atom sample 1 cm long and 170 μm wide at a temperature of 25 μK. The interferometer SW, with k vector precisely aligned along $\mathbf{e_x}$, is formed by counter-propagating light E^a and E^b, detuned 120 MHz to the blue side of the $F = 1 \rightarrow F' = 2$ D2 transition. The interferometer SW is pulsed for 300 ns at $t = 0$ and $t = T$ [Fig. 1(b)], with typical pulse area $\Theta \approx 1.5$ at less than 3% spontaneous scattering probability. The total interrogation time $2T$ is chosen to be 6.066 ms or 12.165 ms.

The AQKR pulses are delivered by a different standing wave that is formed by retroreflecting a traveling laser beam that is 6.8 GHz detuned to the red side of the $F = 1 \rightarrow F' = 2$ D2 transition, and is 40 mrad misaligned from the $\mathbf{e_x}$ direction. The projection of AQKR k vector along the interferometer SW direction $\mathbf{e_x}$ gives $(\omega_Q - \omega_{Q'})/\omega_Q \sim 1.6 \times 10^{-3}$ that will be ignored in this Letter [17]. The SW field is pulsed at $t = T_i$ according to Eq. (1) [Fig. 1(b)], with 500 ns duration and has a typical pulse area $\theta \sim 0.1$–1.3. Our previous work has shown that the magnetic confinement introduces negligible perturbation to the matter wave interference along $\mathbf{e_x}$ [19,20]. Here we take advantage of the confinement to maintain the 170 μm transverse atomic sample distribution within the 2-mm-diameter of the AQKR laser beam, allowing very consistent AQKR interactions for time longer than 6 ms. The "grating echo" signal amplitude is retrieved at around $t = 2T$ using a heterodyne technique [14,19], and recorded in repeated experiments as chosen parameters of AQKR are scanned. To obtain $f = f(\theta, \{T_i\})$, we normalize the grating echo amplitude with the amplitude when no AQKR pulse is applied. The half-Talbot time $T_{1/2} \approx 33.2 \mu$s and the pulse area θ are estimated by comparing experimental data with Eq. (3). Since θ is proportional to the SW intensity, we determine the relative magnitudes of θ at different SW intensities with a photodiode.

To verify the fidelity saturation predicted by Eq. (4), we fix the pulse separation at $T_{1/2} = 33.2 \mu$s (normalized kicking period $\tau = \omega_Q T_{\text{kick}} = \pi$), the perturbation

strength $\phi = 2\theta \sin(\omega_Q T_{\text{start}})$, and collect the normalized interferometer output f as a function of the number of kicked rotor pulses N. Figure 3(a) shows four scatter plots for $\phi = 0.6, 1.1, 1.5, 2.1$ and $1 \leq N \leq 60$. Here each ϕ corresponds to a different T_{start} at a fixed $\theta = 1.22(10)$, which was determined by comparing the photodiode readouts with those from other experiments, as will be described below. The solid curves are derived from Eq. (4) in the absence of free parameters. From Fig. 3(a) we see a partial loss, revival, and saturation of f with increasing N for all strengths ϕ. One can see from the figure that the loss and revival of coherence at small N happens more rapidly as ϕ increases. For $\phi = 2.1$, the normalized interferometer output f at $N = 3$ is almost equal to the saturation value.

Having confirmed that the coherence of the interferometer as a function of the number of applied kicks N shows a revival and approach to a finite asymptote, we study this asymptotic coherence as a function of the perturbation strength ϕ by varying T_{start} at a fixed large number of kicks. Typical results are shown in Fig. 3(b) again for the case where $\theta = 1.22$, together with a solid curve by Eq. (4) evaluated at $N \rightarrow \infty$. The data for $N = 20$ kicks [circles, Fig. 3(b)] match the asymptotic theoretical curve very well (see Fig. 2 in Ref. [5]) over the achieved range of $0 < \phi < 2.44(20)$. For as many as $N = 150$ kicks [triangles, Fig. 3(b)], we only observe a 40%, T_{start}-independent decrease of the interferometer signal. This additional coherence loss is likely related to our experimental imperfections, including losses and transverse excitations of guided atoms induced by the large number of kicks. We also plot the same data directly vs T_{start} in the inset of Fig. 3(b), which exhibits recoil frequency oscillations as expected from Eq. (4).

To illustrate the periodic dependence of the saturation effect on T_{kick}, we plot the normalized interferometer output, f, as a function of both τ and N in Fig. 4. The density plot in Fig. 4(a) composes 40×80 data points, which scan $0.42\pi \leq \tau \leq 2.6\pi$, and $1 \leq N \leq 40$. [The value of f vs N at $\tau = \pi, 2\pi$ in Fig. 4(a) provides the type of plots in Fig. 3(a)]. At a fixed τ, Fig. 4 shows that f generally
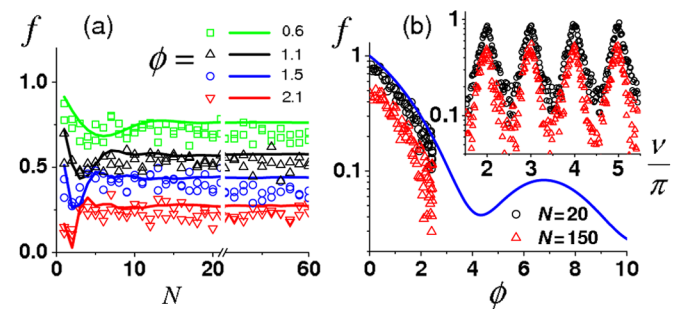

FIG. 3 (color online). Normalized interferometer output f at $\tau/\pi = 1$. Scatter plots give experimental data. Solid lines are calculated according to Eq. (4). (a) f vs N. (b) f vs ϕ. The inset gives the same experimental data plotted vs ν/π; here $\nu = \omega_Q T_{\text{start}}$.
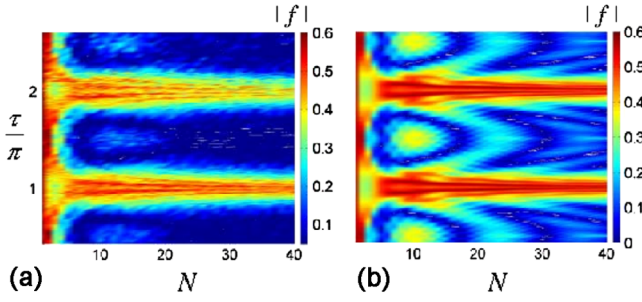
FIG. 4 (color online). (a) Normalized interferometer output $|f|$ with τ/π and N. Here $\omega_Q T_{\text{start}}/\pi = 0.5$. (b) Simulation of $|f|$ using Eq. (3) with $\theta = 0.7$.

reduces from unity at $N = 0$ to zero as N increases. However, we see multiple bright fringes of high f value that, with increasing N, become more narrowly confined around the quantum resonances $\tau = \pi, 2\pi$ without significant decay. Here the SW pulse area is estimated to be $\theta = 0.7$ by comparing the measured f with Eq. (3), with which we obtain the simulation results in Fig. 4(b). The two figures show good agreement both for small N, and for τ around $\pi, 2\pi$. Details of the features in the plot near the quantum resonances vary with T_{start} [12]. The origin of the discrepancies at τ far away from $\pi, 2\pi$ is not yet clear, but may be related to the increased energy transfer between the guided atoms and the pulsed SW when the quantum resonance condition is not met [10].

By relating atom interferometer coherence loss with fidelity decay of matter waves under a momentum displacement perturbation, we have presented the first experimental study of matter wave fidelity decay in a δ-kicked rotor potential [4]. Because of the momentum displacement and the resulting spatial displacement between the interferometer paths, a loss of matter wave coherence in the spatially varying AQKR potential could be expected. However, the revival and saturation of the coherence to a nonzero asymptote, as predicted by Ref. [5] in a similar context, is very counterintuitive semiclassically [4] if the corresponding classical motion is chaotic [18] and the perturbation is nonzero. We have shown, with a full quantum treatment, that the saturation of the fidelity is due to the localization of wave coherence scattered by AQKR kicks in a network [Fig. 2(b)]. The effect is also related to the stability of a "pseudoclassical standard map" [5,21], as seen by evaluating Eq. (3) near quantum resonances.

Previous experimental investigations on AQKR have mostly addressed the evolution of the atomic momentum distribution [10]. It can be shown that the fidelity saturation effect observed in this Letter is accompanied with a certain distribution of the matter wave correlation function $W(P, X)$, which is invariant under the iteration given in Eq. (2) induced by each AQKR kick [22]. This invariant distribution of matter wave coherence complements the stable momentum distribution near quantum resonances [10,21,23], and may be further explored for applications in interferometric measurements.

*swu@umd.edu

[1] A. Peres, Phys. Rev. A **30**, 1610 (1984).
[2] A. Jalabert *et al.*, Phys. Rev. Lett. **86**, 2490 (2001); F. Cucchietti *et al.*, Phys. Rev. Lett. **91**, 210403 (2003).
[3] T. Prozen *et al.*, Phys. Rev. Lett. **94**, 044101 (2005); T. Gorin *et al.*, Phys. Rep. **435**, 33 (2006).
[4] C. Petitjean *et al.*, Phys. Rev. Lett. **98**, 164101 (2007).
[5] S. Wimberger *et al.*, J. Phys. B **39**, L145 (2006).
[6] F. Haug *et al.*, Phys. Rev. A **71**, 043803 (2005).
[7] H. M. Pastawski *et al.*, Phys. Rev. Lett. **75**, 4310 (1995); N. Friedman *et al.*, Phys. Rev. Lett. **86**, 1518 (2001); S. Schlunk *et al.*, Phys. Rev. Lett. **90**, 054101 (2003); M. Andersen *et al.*, Phys. Rev. Lett. **97**, 104102 (2006).
[8] Previous atom interferometry experiments have illustrated how decoherence emerges as soon as "whichway information" is generated due to the coupling between the atom with the environmental degrees of freedom. For example, M. Chapman *et al.*, Phys. Rev. Lett. **75**, 3783 (1995); H. Uys *et al.*, Phys. Rev. Lett. **95**, 150403 (2005).
[9] *Atom Interferometry*, edited by P. R. Berman (Academic Press, Cambridge, 1997).
[10] For example, F. Moore *et al.*, Phys. Rev. Lett. **75**, 4598 (1995); C. Ryu *et al.*, Phys. Rev. Lett. **96**, 160403 (2006).
[11] B. V. Chirikov, Phys. Rep. **52**, 263 (1979).
[12] A. Tonyushkin *et al.*, Phys. Rev. A **79**, 051402(R) (2009).
[13] F. M. Izrailev and D. L. Shepelyanskii, Teor. Mat. Fiz. **43**, 417 (1980) [Theor. Math. Phys. **43**, 553 (1980)]; F. M. Izrailev *et al.*, Theor. Math. Phys. **43**, 553 (1980).
[14] S. B. Cahn *et al.*, Phys. Rev. Lett. **79**, 784 (1997); D. Strekalov *et al.*, Phys. Rev. A **66**, 023601 (2002).
[15] J. F. Clauser *et al.*, Appl. Phys. B **54**, 380 (1992).
[16] $W(P, X)$ is referred to as Weyl function. See S. Chountasis and A. Vourdas, Phys. Rev. A **58**, 848 (1998); S. Wu, P. Striehl, and M. G. Prentiss, arXiv:0710.5479.
[17] With L the length of atomic sample along x, we assume $(Q - Q')L \gg 1$ so that a distinction between the diffractions due to the interferometer SW and the kicked rotor SW can be made. On the other hand, $(\omega_Q - \omega_{Q'})NT_{\text{kick}} \ll 1$ is required for Eq. (4) to be approximately valid. Both requirements are satisfied in this work.
[18] The classical motion of atoms is controlled by the parameter $K = 2\theta\omega_Q T_{\text{kick}}$. Nearly complete chaos (i.e., with nearly no stable orbit in phase space) emerges for $K > 4$ [10,11].
[19] S. Wu, Ph. D. thesis, Harvard University, 2007.
[20] S. Wu *et al.*, Phys. Rev. Lett. **99**, 173201 (2007); E. J. Su *et al.*, arXiv:physics/0701018.
[21] S. Fishman *et al.*, Phys. Rev. Lett. **89**, 084101 (2002).
[22] To see this, one needs to evaluate the sum in Eq. (3) with general r_N and s_N. This will be given in a future publication.
[23] C. F. Bharucha *et al.*, Phys. Rev. E **60**, 3881 (1999).
[24] R. Friedberg *et al.*, Phys. Rev. A **48**, 1446 (1993).